IEEE Photonics Journal
An IEEE Photonics Society Publication

Open Access

In-Line Fiber Michelson Interferometer for Enhancing the Q Factor of Cone-Shaped Inwall Capillary Coupled Resonators

Volume 10, Number 2, April 2018

Xiaobei Zhang, ***Member, IEEE***
Huawen Bai
Haiyang Pan
Jiawei Wang
Ming Yan
Hai Xiao
Tingyun Wang

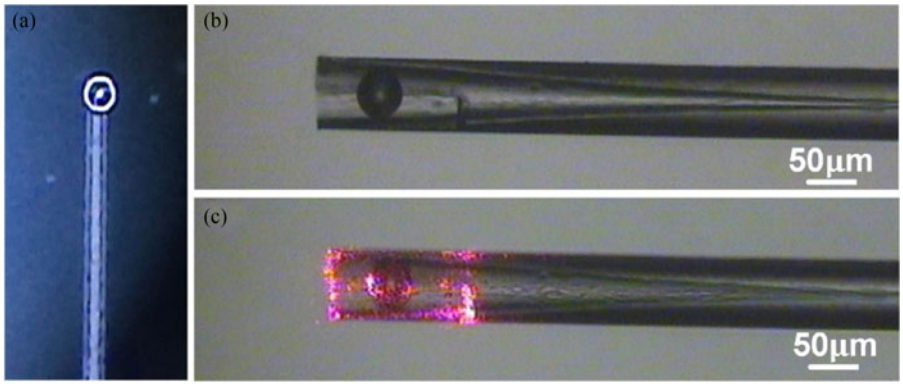

DOI: 10.1109/JPHOT.2018.2818715
1943-0655 © 2018 IEEE

IEEE photonics SOCIETY
IEEE

In-Line Fiber Michelson Interferometer for Enhancing the Q Factor of Cone-Shaped Inwall Capillary Coupled Resonators

Xiaobei Zhang,[1] ***Member, IEEE***, **Huawen Bai**,[1] **Haiyang Pan**,[1] **Jiawei Wang**,[1] **Ming Yan**,[1] **Hai Xiao**,[2] **and Tingyun Wang** [1]

[1]Key Laboratory of Specialty Fiber Optics and Optical Access Networks, Joint International Research Laboratory of Specialty Fiber Optics and Advanced Communication, Shanghai Institute for Advanced Communication and Data Science, Shanghai University, Shanghai, 200444, China
[2]Department of Electrical and Computer Engineering, Clemson University, Clemson, SC 29634 USA

DOI:10.1109/JPHOT.2018.2818715
1943-0655 © 2018 IEEE. Translations and content mining are permitted for academic research only. Personal use is also permitted, but republication/redistribution requires IEEE permission. See http://www.ieee.org/publications_standards/publications/rights/index.html for more information.

Manuscript received January 10, 2018; revised March 11, 2018; accepted March 20, 2018. Date of publication March 23, 2018; date of current version April 11, 2018. This work was supported by the National Natural Science Foundation of China under Grants 61675126 and 61377081 and by the Natural Science Foundation of Shanghai. Corresponding author: X. Zhang (e-mail: xbzhang@shu.edu.cn).

Abstract: An in-line fiber Michelson interferometer in a cone-shaped inwall capillary with the whispering gallery mode microsphere resonator integrated inside is demonstrated for enhancing the Q factor, which is fabricated on the etched capillary by the femtosecond laser micromachining to decrease the coupling paths. The modulated symmetric WGM resonances and asymmetric Fano resonances induced by the Michelson interferometer are observed in the reflection spectra, with a slope of 91.87 dB/nm and Q factor as 3.85×10^4 achieved. Numerical simulations with the transfer matrix method also validate the resonator spectra modulated by the Michelson interference. This method shows a perspective potential for the enhancement of the Q factor by tailoring interacting paths through the femtosecond laser micromachining.

Index Terms: Optical fiber sensors, resonator, fiber optics, optical device fabrication.

1. Introduction

Whispering gallery mode (WGM) resonators [1], [2] are usually inherently owning symmetrical Lorentzian line shapes, with wide application potentials in the fields of sensing [3]–[11] and lasing [12]–[15]. Compared to Lorentzian line shapes, asymmetrical Fano line shapes [16]–[20] and electromagnetically induced transparency (EIT) [21] have also attracted a great level of interests. Meanwhile, configurations for coupling the light in or out are important, critical and essential for resonators, while the *Q* factor is the most significant parameter. Usually, we can utilize prism or fiber taper to excite the WGM via the overlap of the evanescent fields [22]. The first method using the prism coupler has a higher coupling efficient [23]. But it requires bulk components, which results into the difficulties to integrate. The other method is to control the distance between the fiber taper and microsphere [24], while the fiber tapers are fragile. Some other schemes, such as using free-space directly coupling method [25], [26], the D-fiber [27] or side polished fiber [28], are still bulky and not easy to be integrated for applications. Besides coupling structures mentioned above,

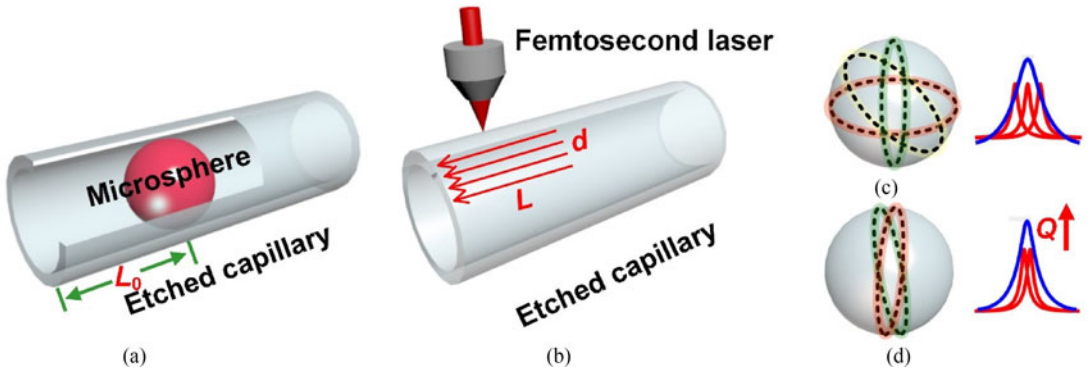

Fig. 1. (a) Schematic of the in-line fiber Michelson interferometer integrated with a WGM resonator. (b) Process of the femtosecond laser micromachining. (c) Lots of coupling paths exist in the uninscribed coupler. (d) Less coupling paths obtained in the inscribed coupler.

chaos-assisted broadband momentum transformation in optical microresonators is proposed and demonstrated recently [29].

Some novel coupling structures in the form of in-line fiber couplers have been reported, which shows the merits such as the compact size and potential for integration. A microsphere is immersed into a chemical etched photonic crystal fiber [30], of which the coupler is robust and compact with the Q factor of 1.58×10^4. A polymer microsphere is encapsulated into the capillary of a micro structured optical fiber [31], in direct contacting with the guiding core, with the Q factor of about 0.22×10^4. An in-fiber Mach-Zehnder interferometer and WGM sphere resonator coupling structure [32], is demonstrated by the femtosecond laser micromachining with the Q factor of about 0.54×10^4. Recently, we propose and demonstrate a cone-shaped inwall coupler for excitation of the WGM of a microsphere resonator, which has the advantages such as the reflective type, alignment-free and mechanically robust [33]. Because the WGM resonator produces many touching points between the capillary and the microsphere, there are many paths excited and therefore the Q factor is limited. Thanks to the femtosecond laser micromachining, the coupling points would be straightforward decreased if a rectangle notch can be inscribed on the etched capillary.

In this letter, we report an in-line fiber Michelson interferometer integrated with a WGM resonator to enhancing the Q factor. A high-index microsphere is embedded into the in-line fiber Michelson interferometer to excite the WGM resonances. Lorentzian line shape and Fano resonances are observed in the reflection spectra with the Michelson interference. Less WGM paths are excited as the existence of the notch, hence the Q factor of WGM resonance and the slopes of the Fano resonance increase. Therefore, the device realizes an alignment free integrated lab-in-fiber platform for WGM excitation, also achieving a solution for enhancing the Q factor.

2. Experimental Setup

Fig. 1(a) shows the schematic of the in-line fiber Michelson interferometer integrated with a WGM resonator, which is simply fabricated by the chemically etching and femtosecond laser micromachining, with L_0 denoted as the distance from the capillary end to the coupling point. The preliminary fabrication processes have been described in detail [33]. Then, a rectangle notch is fabricated by the femtosecond laser micromachining [34], as shown in Fig. 1(b). A Ti: Sapphire laser pulses with a wavelength of 800 nm, pulse width of 120 fs and repetition frequency of 1 kHz are focused on the surface of the end of the etched capillary by the microscope objective. The numerical aperture (NA) of the objective lens is 0.42, and the average power of pulse before entering the objective lens is adjusted as 5 mW. The capillary is manipulated by a computer-controlled translation stage. The route is set as a rectangle shape with the length as L and the width as d. The start point on the surface of the capillary is away from the end of the capillary. The route is swept from the start point to the end of the capillary with the moving speed as 3 μm/s, and then move back to a new

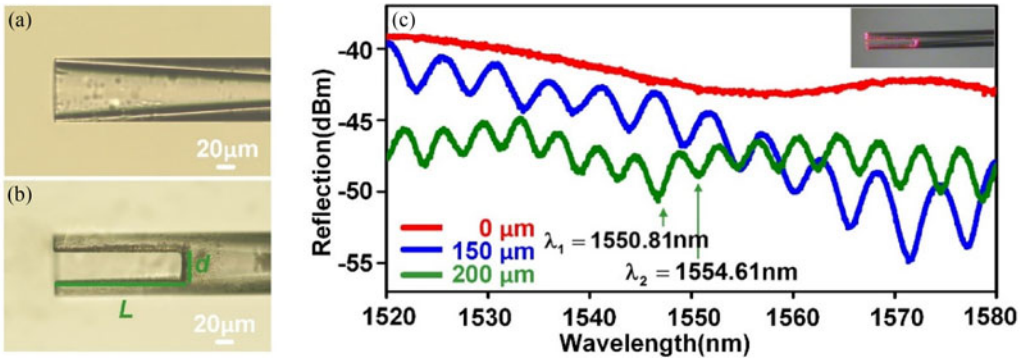

Fig. 2. (a) Microscope image of the cone-shaped inwall capillary after the etching. (b) Microscope image of the etched cone-shaped inwall capillary after the femtosecond laser micromachining (L = 150 μm and d = 35 μm). (c) Reflection spectra of the coupler with the inscribing length L as 0 μm (red, for the case without the notch), 150 μm (blue) and 200 μm (green), respectively. The inset shows the device illuminated by a red laser.

start point. After each route, the fabrication process repeats again, as shown in the Fig. 1(b). If the width of the coupler is about 40 μm, 8 times is necessary for the sweeping process. Finally, the WGM coupler can be obtained and then cleaned using the ultrasonic. Both the whole process and the sample morphology are in-situ monitored by a CCD camera in real time, which makes the fabrication simple and precise. As shown in Fig. 1(c), massive coupling paths would form a WGM resonance with a relative smaller *Q* factor. Fig. 1(d) describes the coupling paths after the femtosecond laser inscribing and hence the *Q* factor increases, as the full width at half-maximum (FWHM) decreases.

Fig. 2(a) and (b) show the microscope images of the coupler before and after the femtosecond laser micromachining, respectively, with *L* as 150 μm and *d* as 35 μm. Fig. 2(c) shows the interference reflections of the coupler with the rectangle length of 0 μm, 150 μm and 200 μm inscribed by the femtosecond laser system. The inset is the microscopic image of the coupler illuminated with a red laser. It can be seen clearly that, there are bright areas on the rectangle shape, which indicate that there are two mainly partial reflections that forms the Michelson interference pattern. In Fig. 2(c), the red line is the reflection of the origin coupler without the femtosecond laser micromachining processing, while blue and green lines are the reflections of the inscribed coupler with different inscribing lengths. The free spectral range $FSR = \lambda_2 - \lambda_1 = \lambda_1\lambda_2/(2n_{cap}L)$ [λ_1 and λ_2 in Fig. 2(c)] proves that the interference pattern is the spectrum of a Michelson cavity with the different cavity lengths. And we can also get the normalized complex reflection t_M of the Michelson interferometer as the following [35].

$$t_M = r\left(\frac{\varphi}{2\pi} + \frac{2\pi - \varphi}{2\pi}\exp(2i\delta_m)\right) \tag{1}$$

where $\delta_m = 2\pi n_{cap}L/\lambda$ is the phase difference of the Michelson interferometer. φ is the inscribed angle in contrast to the whole coupler as shown in Fig. 3(c). *r* is the reflection coefficient at the capillary-air interface given by $r = (n_{cap} - n_{air})/(n_{cap} + n_{air})$. n_{cap} and n_{air} are the refractive indices of capillary and air, respectively. And λ is the wavenumber in vacuum.

To investigate the characteristics of the coupler in details, two parameters are introduced. The contrast ratio (CR), which indicates the difference of the ordinate values of the maximum and minimum of the Michelson interferometer spectrum, also reveals the quality of the coupler. The average reflection power (ARP), which describes the reflection power of the input through the coupler, can also indicate the loss of the Michelson interferometer. Fig. 3(a) and (b) show the couplers with the width *d* of 20 μm and 40 μm, respectively. The inset of Fig. 3(c) shows the microscope image of the cross section of the coupler in Fig. 3(a), respectively. The relationships with $sin(\varphi/2) = d/2R_0$ could be obtained from the schematic image, with R_0 as the inner radius of the

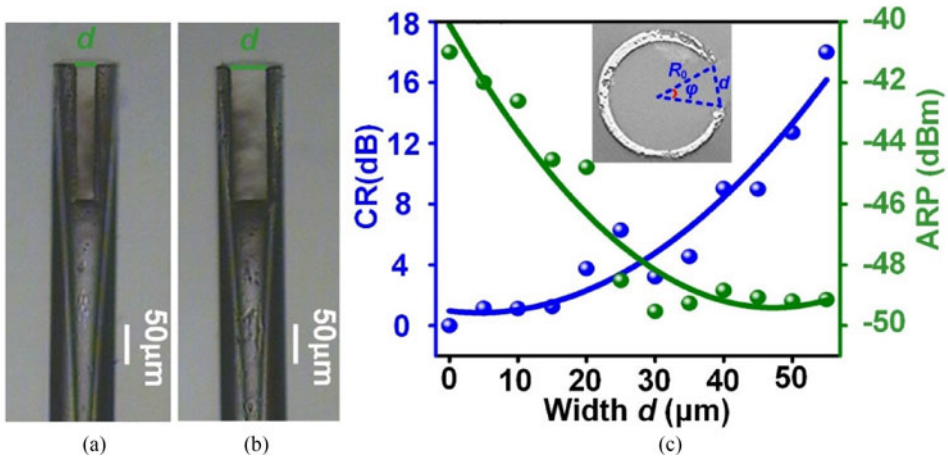

Fig. 3. (a) and (b) are the devices with the inscribing width d as 20 μm and 40 μm, respectively, and L = 150 μm. (c) ARP and CR as functions of the width d. The inset shows the cross section of device and definitions.

capillary. The Optical Sensing Analyzer (Si725) is used to record the changes of the ARP and CR under different widths. The percentage of the two reflections of the Michelson interference varies as the width *d* changes. As shown in Fig. 3(c), the ARP decreases as the width d increases. This result is mainly caused by the femtosecond laser inscribing process, which converts the etched capillary to be a Michelson Interferometer. The larger the width is, the more the inscribing area is. When the input passes through the coupler and reflects back, the power has more loss, so the APR decreases. $d = 0$ indicates that the capillary has not been inscribed, and the optical loss is lower than the inscribed devices. The CR increases as the width *d* increases. The reason is that, the scale of the one reflective light path increases, and the other path decreases in the Michelson interferometer as the width *d* increases. The interference between the two light paths reaches its maximum value theoretically when $\varphi = \pi$

3. Results and Analysis

The previous work has modeled and investigated the Fano resonances in the cone-shaped inwall capillary based microsphere resonator [33], [36], using the normalized reflection with the transfer matrix method (TMM). Similarly, the transmission model here can be modified as there exists a Michelson interference with two parts, of which the normalized reflection T_R can be rebuilt as the following.

$$T_R = \left| \frac{2\pi - 2\varphi}{2\pi} \left(r\left(\frac{t - \tau t p^2}{1 - \tau t^2 p^2} \right)^2 \exp(2i\delta) - \frac{\sqrt{\tau} k^2 p}{1 - \tau t^2 p^2} \right) + \frac{\varphi}{2\pi} r \left(\frac{t - \tau p^2}{1 - \tau t p^2} \right)^2 \right.$$
$$\left. \exp(2i\delta) + \frac{\varphi}{2\pi} r(\exp(2i\delta - 2i\delta_m)) \right|^2 \quad (2)$$

where $\varphi/2\pi$ is the ratio of the inscribing part relative to the whole capillary. δ is the phase difference induced by the distance L_0. t and k are the transmission coefficient and coupling coefficient of the capillary-resonator system. τ is the resonator round-trip transmission coefficient. p is halfway phase factor satisfying $p = exp(i2\pi^2 n_{\text{eff}} R/\lambda)$. n_{eff} and R is the effective index and the radius of the microsphere.

Theoretical analysis can be performed based on the model described by (2). As seen in Fig. 4(a), there are two parts in the model of (2), where ② and ③ correspond to the model of Fig. 4(b), of which the theory has been investigated. ①and ④correspond to the model of Fig. 4(c),

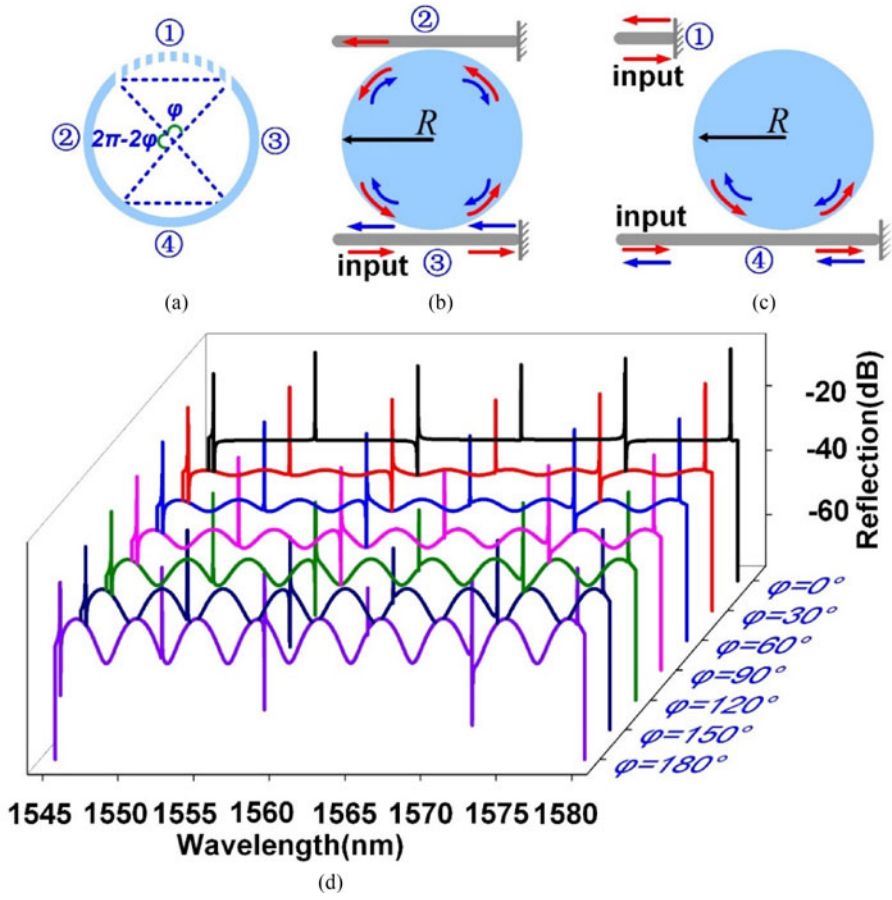

Fig. 4. (a) The cross section of the modeling. (b) and (c) are the schematics of the two parts in (2). (d) Variation of the reflection spectra with φ from 0 to 180 degree.

which is the Michelson model with a microsphere. Simulation parameters are chosen as $r = 0.2$, $L = 200\,\mu$m, $L_0 = 30\,\mu$ m and φ from 0 to 180 degree. Fig. 4(d) shows the variations of the reflection spectra with variations of φ under $t = \tau = 0.9998$. Firstly, the resonance with different line shapes are superimposed on the background of Michelson interference pattern. Secondly, the CR of the Michelson resonance increases with the φ increasing which agrees well with the experiments in Fig. 2(c). Theoretically, the coupling paths decreases as the width d increases, and the WGM has higher Q factor.

In the demonstration experiment, the microsphere is made of Barium Titanite glass with a refractive index as 1.93, of which the diameter is around 45 μm. This makes it easily inset into the end of the coupler but not achieve the side of rectangle notch. In the process of insetting the microsphere, one of the six-axis translation stage is used to fix the coupler and another is to fix a fiber taper adhering the high refractive index microsphere. Then we move the second six-axis translation stage to the first one and insert the microsphere into the end face of the coupler precisely. Fig. 5(a) shows the microscope image of fiber taper adhering the high refractive index microsphere. After removing the fiber taper, the microsphere remains stable inside the coupler, as shown in Fig. 5(b). Fig. 5(c) is the microscope image of the coupler illuminated with a red laser. No changes are observed in the reflection spectrum when the microsphere is not closely fitted in the capillary. When the microsphere is inserted into the coupler firmly, we could observe the spectrum changing through the Optical Sensing Analyzer in real time, while the whole process is monitored by a CCD camera.

The Optical Sensing Analyzer inherently contains a tunable laser, a circulator and an optical spectrum analyzer. The wavelength range is from 1510 nm to 1590 nm, and the resolution is 5 pm.

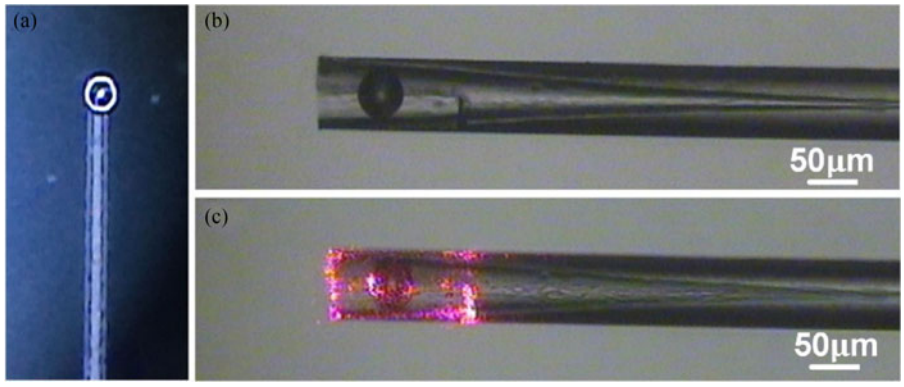

Fig. 5. (a) Microscope image of fiber taper adhering a high refractive index microsphere. (b) Microsphere inserted into the coupler. (c) Microscope image of the coupler illuminated with a red laser.

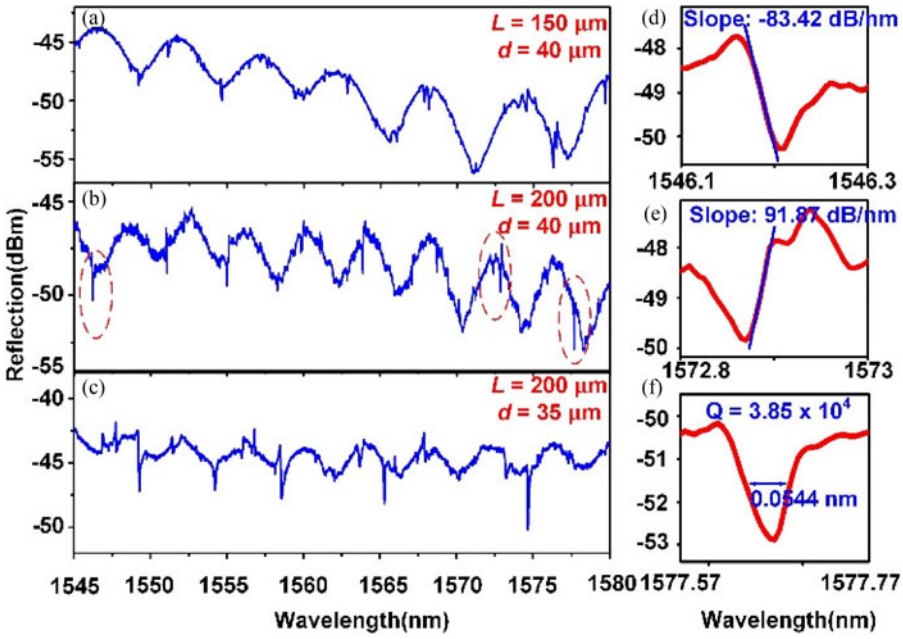

Fig. 6. Reflection spectra of the devices with different inscribing Michelson interferometer lengths and widths. (a) $L = 150\,\mu$m, $d = 40\,\mu$ m. (b) $L = 200\,\mu$ m, $d = 40\,\mu$ m. (c) $L = 200\,\mu$m, $d = 35\,\mu$m. (d) and (e) Asymmetric Fano resonances with slopes as -83.42 dB/nm and 91.87 dB/nm, respectively. (f) Symmetric Lorentzian line shape with the Q factor of 3.85×10^4.

Fig. 6(a) and (b) show the reflection spectra when the couplers of the inscribed length of 150 μm and 200 μm, while widths are the same as 40 μm. In the reflection spectra, the WGM of the microsphere is excited and modified by the Michelson interference pattern. Not only the symmetric Lorentzian line shapes, but also the asymmetric Fano resonances at different wavelength can be observed, which agree well with the theoretical simulation. The average reflection power decreases when the Michelson interferometer length increases. The longer the inscribing length is, the more the inscribing area is, and the average reflection power would decrease. Fig. 6(b) and (c) show the reflection spectra when the couplers of the inscribed widths of 40 μm and 35 μm, respectively, while their inscribing lengths are both 200 μm. The width of 40 μm has larger loss but higher Q factors and higher slopes can be obtained. This comparison dedicates that appropriately increasing width could decrease the coupling paths effectively, which increases the Q factor and the slope of the Fano resonance. However, the loss would increase when the inscribing width increases,

which suggests that there is a trade-off between the loss and the Q factor. Fig. 6(d)–(f) are the magnifications in spectra of three typical cases. Fig. 6(d) shows the asymmetric Fano resonance with the slope as −83.42 dB/nm. Fig. 6(e) shows the asymmetric Fano resonance with the slope as 91.87 dB/nm. Fig. 6(f) shows the symmetric Lorentzian line shape with the FWHM of 0.0544 nm and Q factor of 3.85×10^4. Compared with the Q factor and slope, the enhancement by the femtosecond laser micromachining is demonstrated and verified.

4. Conclusion

In conclusion, we have presented an in-line fiber Michelson interferometer integrated with a WGM resonator, which is fabricated by chemical etching and femtosecond laser micromachining. The advantages of introducing the rectangular notch is to decrease the coupling paths of WGM from capillary to microsphere. The experiment results prove the theory analysis based on the transfer matrix method. The slope of 91.87 dB/nm and Q factor with 3.85×10^4 are achieved in the reflection spectra, which demonstrate the potential of decreasing the coupling paths for enhancing the Q factor, compared to the work without femtosecond laser micromachining process [33]. The Q factor can be also greatly enhanced by replacing the microsphere with a microdisk [7], as there is only one narrow orbital coupling path, which would also further improve the characteristics of cone-shaped inwall capillary-based microsphere resonators in applications of sensing and lasing.

References

[1] V. S. Ilchenko and A. B. Matsko, "Optical resonators with whispering-gallery modes-part II: Applications," *IEEE J. Sel. Topics Quantum Electron.*, vol. 12, no. 1, pp. 15–32, Jan./Feb. 2006.

[2] A. B. Matsko and V. S. Ilchenko, "Optical resonators with whispering-gallery modes-part I: Basics," *IEEE J. Sel. Topics Quantum Electron.*, vol. 12, no. 1, pp. 3–14, Jan./Feb. 2006.

[3] M. R. Foreman, J. D. Swaim, and F. Vollmer, "Whispering gallery mode sensors," *Adv. Opt. Photon.*, vol. 7, no. 2, pp. 168–240, 2015.

[4] J.-P. Laine, C. Tapalian, B. Little, and H. Haus, "Acceleration sensor based on high-Q optical microsphere resonator and pedestal antiresonant reflecting waveguide coupler," *Sens. Actuators A, Phys.*, vol. 93, no. 1, pp. 1–7, Aug. 2001.

[5] J. Liao, X. Wu, L. Liu, and L. Xu, "Fano resonance and improved sensing performance in a spectral-simplified optofluidic micro-bubble resonator by introducing selective modal losses," *Opt. Exp.*, vol. 24, no. 8, pp. 8574–8580, 2016.

[6] S. Liu *et al.*, "Whispering gallery modes in a liquid-filled hollow glass microsphere," *Opt. Lett.*, vol. 42, no. 22, pp. 4659–4662, 2017.

[7] T. Ma *et al.*, "Simultaneous measurement of the refractive index and temperature based on microdisk resonator with two whispering-gallery modes," *IEEE Photon. J.*, vol. 9, no. 1, Feb. 2017, Art. no. 6800913.

[8] L. Shi, T. Zhu, D. Huang, and M. Liu, "Thermo–optic tuning of integrated polymethyl methacrylate sphere whispering gallery mode resonator," *IEEE Photon. J.*, vol. 8, no. 5, Oct. 2016, Art. no. 2701307.

[9] F. Vollmer and S. Arnold, "Whispering-gallery-mode biosensing: Label-free detection down to single molecules," *Nat. Methods*, vol. 5, no. 7, pp. 591–596, 2008.

[10] Y.-Z. Yan *et al.*, "Robust spot-packaged microsphere-taper coupling structure for in-line optical sensors," *IEEE Photon. Technol. Lett.*, vol. 23, no. 22, pp. 1736–1738, Nov. 2011.

[11] Z. Yang, Y. Wu, X. Zhang, W. Zhang, P. Xu, and S. Dai, "Low temperature fabrication of chalcogenide microsphere resonators for thermal sensing," *IEEE Photon. Technol. Lett.*, vol. 29, no. 1, pp. 66–69, Jan. 2017.

[12] M. Cai, O. Painter, K. J. Vahala, and P. C. Sercel, "Fiber-coupled microsphere laser," *Opt. Lett.*, vol. 25, no. 19, pp. 1430–1432, 2000.

[13] S. M. Spillane, T. J. Kippenberg, and K. J. Vahala, "Ultralow-threshold Raman laser using a spherical dielectric microcavity," *Nature*, vol. 415, pp. 621–623, 2002.

[14] A. Sulaiman, S. W. Harun, and H. Ahmad, "Erbium-doped fiber laser with a microfiber coupled to silica microsphere," *IEEE Photon. J.*, vol. 4, no. 4, pp. 1065–1070, Aug. 2012.

[15] Y. Wang, H. Li, L. Zhao, Y. Liu, S. Liu, and J. Yang, "Tunable whispering gallery modes lasing in dye-doped cholesteric liquid crystal microdroplets," *Appl. Phys. Lett.*, vol. 109, no. 23, 2016, Art. no. 231906.

[16] U. Fano, "Effects of configuration interaction on intensities and phase shifts," *Phys. Rev.*, vol. 124, no. 6, pp. 1866–1878, 1961.

[17] F. Lei, B. Peng, Ş. K. Özdemir, G. L. Long, and L. Yang, "Dynamic Fano-like resonances in erbium-doped whispering-gallery-mode microresonators," *Appl. Phys. Lett.*, vol. 105, no. 10, 2014, Art. no. 101112.

[18] B.-B. Li *et al.*, "Experimental controlling of Fano resonance in indirectly coupled whispering-gallery microresonators," *Appl. Phys. Lett.*, vol. 100, no. 2, 2012, Art. no. 021108.

[19] M. F. Limonov, M. V. Rybin, A. N. Poddubny, and Y. S. Kivshar, "Fano resonances in photonics," *Nat. Photon.*, vol. 11, no. 9, pp. 543–554, 2017.

[20] Y. Miao, Y. Peng, Y. Xiang, M. Li, Y. Lu, and Y. Song, "Dynamic fano resonance in thin fiber taper coupled cylindrical microcavity," *IEEE Photon. J.*, vol. 8, no. 6, Dec. 2016, Art. no. 4502806.

[21] X. Zhou, T. Zhang, X. Yin, L. Chen, and X. Li, "Dynamically tunable electromagnetically induced transparency in graphene-based coupled micro-ring resonators," *IEEE Photon. J.*, vol. 9, no. 2, Apr. 2017, Art. no. 6600609.
[22] V. B. Braginsky, M. L. Gorodetsky, and V. S. Ilchenko, "Quality-factor and nonlinear properties of optical whispering-gallery modes," *Phys. Lett. A*, vol. 137, no. 7/8, pp. 393–397, 1989.
[23] M. L. Gorodetsky and V. S. Ilchenko, "Optical microsphere resonators: Optimal coupling to high-Q whispering-gallery modes," *J. Opt. Soc. Amer. B*, vol. 16, no. 1, pp. 147–154, 1999.
[24] M. Cai, O. Painter, and K. J. Vahala, "Observation of critical coupling in a fiber taper to a silica-microsphere whispering-gallery mode system," *Phys. Rev. Lett.*, vol. 85, no. 1, pp. 74–77, 2000.
[25] S. X. Zhang, L. Wang, Z. Y. Li, Y. Li, Q. Gong, and Y. F. Xiao, "Free-space coupling efficiency in a high-Q deformed optical microcavity," *Opt. Lett.*, vol. 41, no. 19, pp. 4437–4440, 2016.
[26] J. Zhu *et al.*, "Interfacing whispering-gallery microresonators and free space light with cavity enhanced Rayleigh scattering," *Sci. Rep.*, vol. 4, 2014, Art. no. 6396.
[27] L. Shi, T. Zhu, D. Huang, M. Liu, M. Deng, and W. Huang, "In-fiber whispering-gallery-mode resonator fabricated by femtosecond laser micromachining," *Opt. Lett.*, vol. 40, no. 16, pp. 3770–3773, 2015.
[28] N. Dubreuil, J. C. Knight, D. K. Leventhal, V. Sandoghdar, J. Hare, and V. Lefèvre, "Eroded monomode optical fiber for whispering-gallery mode excitation in fused-silica microspheres," *Opt. Lett.*, vol. 20, no. 8, pp. 813–815, 1995.
[29] X. Jiang *et al.*, "Chaos-assisted broadband momentum transformation in optical microresonators," *Science*, vol. 358, no. 6361, pp. 344–347, 2017.
[30] R. Wang, M. Fraser, J. Li, X. Qiao, and A. Wang, "Integrated in-fiber coupler for microsphere whispering-gallery modes resonator excitation," *Opt. Lett.*, vol. 40, no. 3, pp. 308–311, 2015.
[31] K. Kosma, G. Zito, K. Schuster, and S. Pissadakis, "Whispering gallery mode microsphere resonator integrated inside a microstructured optical fiber," *Opt. Lett.*, vol. 38, no. 8, pp. 1301–1303, 2013.
[32] L. Shi, T. Zhu, D. Huang, C. Liang, M. Liu, and S. Liang, "In-fiber Mach–Zehnder interferometer and sphere whispering gallery mode resonator coupling structure," *Opt. Lett.*, vol. 42, no. 1, pp. 167–170, 2017.
[33] X. Zhang *et al.*, "Fano resonances in cone-shaped inwall capillary based microsphere resonator," *Opt. Exp.*, vol. 25, no. 2, pp. 615–621, 2017.
[34] X. Zhang *et al.*, "Fabrication and sensing characteristics of intrinsic Fabry–Perot interferometers in fiber tapers," *Chin. Opt. Lett.*, vol. 13, no. 12, pp. 120602–120605, 2015.
[35] L. Yuan *et al.*, "Fiber inline Michelson interferometer fabricated by a femtosecond laser," *Opt. Lett.*, vol. 37, no. 21, pp. 4489–4491, 2012.
[36] X. Zhang *et al.*, "Theoretical aspects and sensing demonstrations of cone-shaped inwall capillary-based microsphere resonators," *Photon. Res.*, vol. 5, no. 5, pp. 516–520, 2017.